

Enhancing Seismic Noise Suppression Using the Noise2Noise Framework

Mitsuyuki Ozawa¹

¹Mitsuyuki Ozawa JGI, Inc

March 05, 2024

Abstract

Although supervised deep learning (DL) offers a potent solution for removing noise from seismic records, challenges are encountered owing to the scarcity of noise-free labels. The innovative Noise2Noise method eliminates the need for clean training targets and extends the applicability of deep learning to seismic data denoising. In this study, we introduce the Noise2Noise Enhancement (N2NE) framework, which improves upon the conventional noise reduction methods used in seismic processing. The applicability of this framework was quantitatively examined using actual field noise under two scenarios: with and without repeated shots. In scenarios with repeated shots, the N2NE framework enhances the conventional stacking method. In addition, the substack strategy, which employs smaller substacks for preliminary noise suppression before DL training, boosts noise suppression. In scenarios without repeated shots, the N2NE framework refines conventional denoising methods (F-X deconvolution) by utilizing information from the common-shot and receiver domains. The N2NE framework lays a foundation for future research on N2N-based seismic denoising methods and contributes to improving the quality of seismic records and the efficiency of data acquisition.

ENHANCING SEISMIC NOISE SUPPRESSION USING THE NOISE2NOISE
FRAMEWORK

Running Title: ENHANCING SEISMIC NOISE SUPPRESSION

Mitsuyuki Ozawa, JGI, Inc.,1-5-21, Otsuka, Bunkyo-ku, Tokyo 112-0012, Japan,

mitsuyuki.ozawa@jgi.co.jp

Original paper date of submission: 2 January 2024

GEOPHYSICS®

ENHANCING SEISMIC NOISE SUPPRESSION USING THE NOISE2NOISE FRAMEWORK

| | |
|------------------------|--|
| Journal: | <i>Geophysics</i> |
| Manuscript ID | Draft |
| Manuscript Type: | Technical Paper |
| Keywords: | machine learning, signal processing, noise, stacking |
| Manuscript Focus Area: | Signal Processing |
| | |

SCHOLARONE™
Manuscripts

ABSTRACT

Although supervised deep learning (DL) offers a potent solution for removing noise from seismic records, challenges are encountered owing to the scarcity of noise-free labels. The innovative Noise2Noise method eliminates the need for clean training targets and extends the applicability of deep learning to seismic data denoising. In this study, we introduce the Noise2Noise Enhancement (N2NE) framework, which improves upon the conventional noise reduction methods used in seismic processing. The applicability of this framework was quantitatively examined using actual field noise under two scenarios: with and without repeated shots. In scenarios with repeated shots, the N2NE framework enhances the conventional stacking method. In addition, the substack strategy, which employs smaller substacks for preliminary noise suppression before DL training, boosts noise suppression. In scenarios without repeated shots, the N2NE framework refines conventional denoising methods (F-X deconvolution) by utilizing information from the common-shot and receiver domains. The N2NE framework lays a foundation for future research on N2N-based seismic denoising methods and contributes to improving the quality of seismic records and the efficiency of data acquisition.

INTRODUCTION

1
2
3
4 Denoising is a crucial step in seismic processing, particularly when seismic records are
5
6
7 contaminated with random and coherent noise. Such noise obscures useful signals (reflections)
8
9
10 and significantly reduces the signal-to-noise ratio (S/N). This degradation in signal fidelity can
11
12
13 result in the misinterpretation of subsurface structures and unreliable results in the inversion
14
15
16 process. To address the challenge of using low-S/N data, various methods have been proposed
17
18
19 over the past several decades to attenuate unwanted noise.
20
21
22
23
24

25 Prediction filter-based methods, including F-X deconvolution (Canales, 1984; Gulunay,
26
27 1986) and polynomial filters (Lu and Liu, 2006; Liu et al., 2011), separate the signal from noise
28
29
30 by utilizing the predictable nature of the seismic signal and the unpredictable nature of noise. For
31
32
33 example, F-X deconvolution exploits the property that a linear or quasi-linear seismic signal in
34
35
36 the t-x domain is equivalent to the predictable superposition of harmonics in the f-x domain. The
37
38
39 median filter (Bednar, 1983) is a widely accepted statistical noise suppression method that
40
41
42 attenuates random noise by selecting a median value within a moving window across the noisy
43
44
45 data. Sparse transformation-based algorithms can convert noisy data into a sparse domain to
46
47
48 selectively attenuate noise using a thresholding coefficient. To achieve this objective, methods
49
50
51 including wavelet (Mousavi et al., 2016), curvelet (Neelamani et al., 2008), seislet (Fomel and
52
53
54
55
56
57
58
59
60

1
2
3
4 Liu, 2010), and radon (Gholami, 2017) transformations with fixed basis functions have proven
5
6 effective. Similarly, decomposition methods, such as singular value decomposition (Bekara and
7
8 van der Baan, 2007), empirical mode decomposition (Bekara and van der Baan, 2009), and
9
10 ensemble empirical mode decomposition (Wang et al., 2012) separate noisy data into modes with
11
12 different frequency bands. The dictionary-learning-based denoising method (Zhu et al., 2015)
13
14 represents seismic data using a set of adaptive basis functions from a learned dictionary. A
15
16 dictionary is typically represented as an explicit matrix involving an iterative training process.
17
18
19
20
21
22
23
24
25
26
27

28 Vertical stacking is the most widely used and reliable denoising technique used for
29
30 seismic processing. The radiant energy of vibroseis is restricted by both equipment limitations
31
32 and the surrounding environment (road conditions and acceptable noise level). Repeated shots at
33
34 the same point are combined to obtain sufficient source energy. The tradeoff between the quality
35
36 of the record and the cost of the survey determines the number of folds. Under specific ideal
37
38 conditions where the signal is consistent and the noise is stationary and random, conventional
39
40 straight stacking, which calculates the arithmetic mean of the signals, ensures complete noise
41
42 reduction. However, these ideal conditions are often not met; consequently, the effectiveness of
43
44 noise reduction through straight stacking is limited. Therefore, diversity stacking, in which each
45
46
47
48
49
50
51
52
53
54
55
56
57
58
59
60

Geophysics

4

1
2
3
4 trace is multiplied and weighted by a scale factor before stacking, is utilized in more complicated
5
6
7 record models.
8
9
10

11 Recent advances in hardware technology have enabled the extensive use of deep learning
12
13 methodologies in a wide range of seismic data processing tasks such as velocity inversion (Yang
14
15 and Ma, 2019), first-arrival picking (Hu et al., 2019), fault detection (Xiong et al., 2018),
16
17
18 deblending (Luiken et al., 2024), and reconstruction (Liu et al., 2021). Deep learning has also
19
20
21 been applied effectively to suppress seismic noise. Deep neural networks (DNNs), particularly
22
23
24 those that use supervised learning algorithms, have demonstrated significant effectiveness.
25
26
27
28
29

30
31 Numerous studies have used extensively labeled datasets for DNN training. These datasets,
32
33
34 which typically consist of paired noisy and noise-free seismic data, are often created
35
36
37 synthetically (Yu et al., 2019; Liu et al., 2018; Dong et al., 2019; Wang et al., 2022) because
38
39
40 acquiring seismic data to serve as noise-free data is practically unfeasible. Although the
41
42
43 supervised method has shown notable effectiveness in denoising synthetic data, its performance
44
45
46 is often degraded when applied to field data, mainly because of the differences between the
47
48
49 synthetic and actual observed data. Several studies (Zhao et al., 2018; Brusova et al., 2021;
50
51
52 Cheng et al., 2023a; Dong et al., 2023) have attempted to enhance network training by extracting
53
54
55
56
57
58
59
60

Geophysics

5

1
2
3
4 noise from the observed field data and integrating it into synthetic data. Although these methods
5
6
7 potentially improve the denoising performance to some degree, a notable data bias remains
8
9
10 between the synthetic and field data. The scarcity of ground truth data has often become a major
11
12
13 challenge in denoising tasks. However, in the field of computer vision, an elegant solution to this
14
15
16 problem called Noise2Noise (N2N) has been developed (Lehtinen et al., 2018). The N2N
17
18
19 strategy utilizes pairs of independent noisy measurements of the same target instead of using
20
21
22 pairs of noisy and clean measurements. Under certain noise distribution conditions, DNNs
23
24
25 trained by N2N can infer clean data. Lapins et al. (2024) met the requirements for independent
26
27
28 pairs of noisy Distributed Acoustic Sensing (DAS) measurements by splicing two fibers hosted
29
30
31 within a single optical cable that recorded the same underlying signal corrupted by different
32
33
34 observational noises. Wang and Zhang (2021) applied N2N to numerical shot data to attenuate
35
36
37 seismic noise and provided a quantitative evaluation compared with conventional denoising
38
39
40 methods such as Band-pass and F-X deconvolution. The most direct method of applying the
41
42
43 Noise2Noise method to seismic data processing is to utilize pairs of repeated raw shot data at the
44
45
46 same point (Shao et al., 2022). However, notably, accessing seismic data is fundamentally
47
48
49
50
51
52
53
54 challenging. Opportunities for processing data before vertical stacking are limited because
55
56
57
58
59
60

1
2
3 vendors typically perform desweeps and vertical stacking automatically to reduce data volume.
4
5
6
7 Therefore, although N2N eliminates the requirement of clean training targets for more practical
8
9
10 applications, researchers have tended to develop N2N-based self-supervised methods that do not
11
12
13 require two independent noisy real measurements for DNN training. An N2N-based denoising
14
15
16 approach with only a single noisy measurement can be achieved through self-supervised
17
18
19 learning, which employs a sampling or subsampling strategy to generate pairs of noisy
20
21
22 measurements (Huang et al., 2021; Shao et al., 2022; Zhao et al., 2023). Some studies have used
23
24
25 conventional seismic denoising methods to provide target data for noisy field data (Yu et al.,
26
27
28 2019; Mandelli et al., 2019; Wang et al., 2019; Shan et al., 2021, Yang et al., 2023). Another
29
30
31 approach is to generate a noisier sample by directly adding noise to already noisy data (Moran et
32
33
34 al., 2020; Zhang et al., 2022; Cheng et al., 2023b; Li et al., 2024). The added noise can be
35
36
37 extracted from observed field data or sampled from a predefined noise distribution based on prior
38
39
40 knowledge. However, while a DNN trained on these noisier samples gains the ability to denoise,
41
42
43 bias exists between noisier and noisy pairs and noise-clean pairs. This bias can significantly
44
45
46 affect DNN denoising performance when applied to noisy raw data. Wang et al. (2023) utilized
47
48
49 high self-similarity in the horizontal direction of common reflection gathers following a normal
50
51
52
53
54
55
56
57
58
59
60

Geophysics

7

1
2
3
4 move-out correction to generate a paired noisy dataset. Song et al. (2023) proposed Shot2Shot
5
6
7 (S2S) with a re-de-noising regularization method, which uses the pair of a shot gather and its
8
9
10 neighboring shot gather for DNN training. The similarity, yet distinct differences, between a shot
11
12
13 gather and its neighbor can lead to a rough estimation result. To address this issue, they
14
15
16
17 incorporated a re-de-noising regularization term into the loss function of the DNN.
18
19
20

21
22 To address the challenge of noise reduction in single noisy measurement scenarios,
23
24 several unsupervised deep learning methods have been developed in addition to the N2N
25
26
27 strategy. Autoencoders (AEs) can preserve subtle data features while removing random noise
28
29
30 through unsupervised learning manner. The denoising ability of AEs has been demonstrated in
31
32
33 seismic domains (Chen et al., 2019; Zhang et al., 2019b; Saad and Chen, 2020; Song et al.,
34
35
36
37 2020). The blindspot strategy (Krull et al., 2019) has been proven to effectively attenuate random
38
39
40
41 noise in seismic data in a self-supervised manner (Birine et al., 2021a, 2021b; Liu et al., 2023;
42
43
44
45 Birine and Ravasi, 2024). Ma et al. (2023) proposed an Attention Cycle GAN Network
46
47
48 (ACGNet) for unpaired training, which was trained using a diverse hybrid training set that
49
50
51 included both noisy and synthetically generated clean data. The model learns the transformation
52
53
54
55 from a noisy domain to a clean domain by focusing on a domain-wide rather than a one-to-one
56
57
58
59
60

1
2
3
4 sample transformation. The Deep Image Prior (DIP) technique (Ulyanov et al., 2020) does not
5
6
7 require labeled clean data for denoising, leveraging the principle that DNNs minimize the loss
8
9
10 function during training by initially fitting predictable signals. Specifically, the structural signals
11
12
13 are more predictive than the unstructured noise signals. In addition, low-frequency components
14
15
16 tend to be predicted before high-frequency components (Rahaman et al., 2019; Xu et al., 2019).
17
18
19 Utilizing these characteristics, the DNN at an optimal number of training epochs focuses on
20
21
22 learning only the coherent and relatively low-frequency signal components, thereby achieving a
23
24
25 denoising effect. Zhang and Wang (2023) demonstrated that a DIP-based recursive denoising
26
27
28 method with improved quality control criteria could effectively attenuate seismic noise.
29
30
31

32
33
34
35 As previously mentioned, several proposed methods have already used conventional
36
37
38 seismic denoising methods to provide target data (henceforth referred to as pseudo-denoised
39
40
41 data) for N2N requirements (Yu et al., 2019; Mandelli et al., 2019; Wang et al., 2019; Shan et al.,
42
43
44 2021; Yang et al., 2023). However, in these studies, conventional denoising methods were solely
45
46
47 utilized in the post-stack domain or common shot domain (CSD). Subsequently, the DNN was
48
49
50 trained in the same domain where denoising was performed by pairing the original noisy data
51
52
53 with the pseudo-denoised data. During the denoising process, noise prediction relies on
54
55
56
57
58
59
60

Geophysics

9

1
2
3
4 information from the applied domain. According to the Universal Approximation Theorem
5
6
7 (Cybenko, 1989), if a DNN is fed with the same information as that used for conventional
8
9
10 denoising, a well-trained DNN can approximate the mapping of these conventional denoising
11
12
13 methods. This implies that the residual noise in pseudo-denoised data can be predicted using the
14
15
16 original noisy data. In reality, owing to the inherent inductive biases in DNNs, which are
17
18
19 particularly noticeable in Convolutional Neural Networks (CNN), and regularization techniques
20
21
22 such as Dropout and Early Stopping, the DNNs do not fully learn from the training data. This
23
24
25 leads to a tendency to preferentially predict more easily predictable signals like the DIP method,
26
27
28 which results in some level of noise reduction. However, this approach causes DNNs to focus on
29
30
31 imitating the results of conventional denoising methods. Consequently, they inherit the
32
33
34 limitations of these methods, resulting in limited improvements in the SNR. Notably, because the
35
36
37 inference phase of the DNN tends to be efficient, this strategy is beneficial for reducing the
38
39
40 computational cost of estimating the denoised gather (Mandelli et al., 2019).
41
42
43
44
45
46
47

48 This study introduced the Noise2Noise enhancement (N2NE) framework, which
49
50
51 improves existing noise reduction methods in seismic processing. We adopted the N2NE
52
53
54 framework under two scenarios: one with repeated shots at the same point and one without. In
55
56
57
58
59
60

1
2
3
4 scenarios involving repeated shots at the same point within the N2NE framework, the DNN was
5
6
7 trained using a pair of repeated data before stacking. N2N enhances the effectiveness of
8
9
10 denoising in traditional stacking techniques by utilizing statistical insights from an entire dataset.
11
12
13 As mentioned earlier, the concept of applying N2N to repeated shots is not novel; however, few
14
15
16 quantitative evaluations have been conducted. This study represents an early attempt to
17
18
19 quantitatively assess the performance of N2N in comparison to conventional stacking methods
20
21
22 for actual field noise. Additionally, we introduced the “substack” strategy as a novel approach to
23
24
25 address extremely noisy data in this case. In a scenario without repeated shots at the same
26
27
28 location within the N2NE framework, existing denoising methods were used to generate pseudo-
29
30
31 denoised data, similar to previous studies. However, the key difference between our N2NE
32
33
34 framework and a previous study is that we employed existing denoising methods within the
35
36
37 common receiver domain (CRD) rather than the CSD. Consequently, the obtained pseudo-
38
39
40 denoised data, including information on adjacent shot points, resulted in residual noise that was
41
42
43 not predictable from the original single-shot data. Therefore, N2N learning can be effective
44
45
46 without directly replicating existing denoising methods. The N2NE framework in these two
47
48
49
50
51
52
53
54
55
56
57
58
59
60

cases was quantitatively evaluated to improve the denoising effectiveness of the existing methods using a pseudo-noise record that added synthetic seismic and field noise data.

METHODS

Noise2Noise Theory

In seismic data processing, the observed seismic data \mathbf{x} are composed of the underlying useful signals \mathbf{s} and additive noise \mathbf{n} , represented as follows:

$$\mathbf{x} = \mathbf{s} + \mathbf{n}. \quad (1)$$

In traditional DNN-based denoising methods, the observed noisy signal \mathbf{x}_i and the corresponding clean signal \mathbf{y}_i are used as the input and output, respectively, for training. The DNNs learn the approximated mapping function f_θ , parameterized by the model weights θ , from noisy data \mathbf{x}_i ground-truth data \mathbf{y}_i by minimizing the expected loss calculated using the loss function \mathcal{L} :

$$\operatorname{argmin}_\theta \sum_i \mathcal{L}(f_\theta(\mathbf{x}_i), \mathbf{y}_i). \quad (2)$$

The N2N framework utilizes the principle that replacing targets with random numbers does not change the estimation as long as their expectations match those of the targets; the estimate remains unchanged (Lehtinen et al. 2018). This implies that training DNNs with observed data \mathbf{x}'_i contaminated by zero-mean noise instead of using ground-truth signals as labels, DNNs can learn noise reduction by minimizing the following equation:

$$\operatorname{argmin}_{\theta} \sum_i \mathcal{L}(f_{\theta}(\mathbf{x}_i), \mathbf{x}'_i). \quad (3)$$

Note that the underlying signals in the \mathbf{x}_i and \mathbf{x}'_i are identical, which means $\mathbf{x}_i = \mathbf{y}_i + \mathbf{n}$, $\mathbf{x}'_i = \mathbf{y}_i + \mathbf{n}'$, where \mathbf{n} and \mathbf{n}' are independent noises.

Processing flow of Repeated Shot Acquisition Scenario

Figure 1 shows a comparison of the processing flows between conventional stacking methods and stacking with the N2NE framework under repeated shot acquisition scenarios. As N2N eliminates the need for clean training targets, we can directly use a pair of repeated shots as training data to optimize the DNN model. In the inference phase, the trained DNN model is applied to each prestacked shot for denoising. The resulting pre-stacked denoised shots are stacked to produce the final denoised shot. Figure 2 shows the processing flow of the N2NE

1
2
3
4 framework for scenarios in which repeated shots were not available. In this scenario, creating a
5
6
7 pseudo-denoised image is necessary. To generate pseudo-denoised data, we employed a
8
9
10 conventional denoising method within the CRD. The DNN model was then trained using pairs of
11
12
13 generated pseudo-denoised shots and original noisy data. Finally, applying the trained DNN to
14
15
16 the original noisy data resulted in a denoised shot that enhanced the noise suppression effect of
17
18
19 the conventional denoising method. In this process, to satisfy the N2N requirement, the residual
20
21
22 noise in the pseudo-denoised shot must be random relative to the original noisy shot. The
23
24
25 pseudo-denoised data generated through the CRD operation included random noise information
26
27
28 from adjacent shots. Therefore, we expect that noise reduction operations in CRD will result in a
29
30
31 higher randomness of the residual noise in relation to the noise in the original data compared
32
33
34 with the CSD operation. Consequently, N2N can be effectively applied to pseudo-denoised data
35
36
37 generated in CRD.
38
39
40
41
42
43
44

45 **Denoising Architecture**

46
47
48

49 For the denoising network, we used the U-shaped fully convolutional network (U-net)
50
51
52 (Ronneberger et al., 2015). Figure 3 shows a schematic of the U-net architecture of the proposed
53
54
55
56
57
58
59
60

Geophysics

14

1
2
3
4 method, which features four encoders (downsampling), four decoders (upsampling), and an
5
6
7 output layer. Each encoder stage comprised a convolutional layer with strides of one (flat
8
9
10 convolution) and two (downsampling convolution). The decoder stages included both a flat
11
12
13 convolutional layer and bilinear upsampling layer. At every downsampling and upsampling
14
15
16 stage, the number of feature maps was doubled and halved, respectively. The initial convolution
17
18
19 layer contained 32 feature maps. Following each convolution, the output underwent batch
20
21
22 normalization (Ioffe and Szegedy, 2015) and was processed using a rectified linear unit (ReLU).
23
24
25 Additionally, skip connections were employed to merge the intermediate outputs of each encoder
26
27
28 stage with the inputs of the corresponding decoder stage, thereby enhancing feature retention.
29
30
31
32
33
34 The final output was obtained after a flat convolution following the encoder and decoder stages.
35
36
37 Throughout the study, the network was optimized to minimize the mean absolute error (MAE)
38
39
40 loss function using the adaptive moment estimation (Adam) optimizer (Kingma and Ba, 2015)
41
42
43 with a learning rate of 1.0×10^{-4} . In all cases, the batch size was set to 2, and the maximum
44
45
46 number of epochs was 200. During the model-training phase, 10% of the dataset was allocated
47
48
49
50 for validation. Early stopping was implemented if the MAE of the validation data did not
51
52
53
54
55
56
57
58
59
60

1
2
3
4 improve after > five consecutive epochs. For implementation, we used the PyTorch framework
5
6
7 and conducted training on a Tesla V100S graphics processing unit.
8
9
10
11
12
13

14 15 EXPERIMENT AND RESULT 16 17 18

19 **Preparing Pseudo-noise data** 20 21 22

23 To conduct a quantitative evaluation, we created pseudo-noise data by combining
24 synthetic seismic data with actual field noise. Synthetic seismic data, which served as the
25 ground-truth signal, were derived from the Marmousi model. Field noise was extracted from
26 downhole monitoring data acquired by the DAS in the Utah FORGE project (Martin and Nash,
27 2019). The pseudo-noise record consisted of 801 shots and 801 receivers, with both the receiver
28 and shot intervals of 25 m in the Marmousi dataset. Although the spatial sampling of the Utah
29 Forge DAS data was 1.02 m, and the sampling intervals were inconsistent relative to the
30 Marmousi model, we combined the two datasets to generate the synthetic noise data,
31 disregarding this discrepancy for simplicity. To evaluate the effect of different noise levels, the
32 field noise was scaled by factors of 0.02, 0.04, 0.08, and 0.16, resulting in an average peak
33 signal-to-noise ratio (PSNR) of the pseudo-noise data with scale factors of 30.93, 24.91, 18.89,
34 and 12.87, respectively. During the DNN training phase, horizontal flip data augmentation was
35 employed to increase the dataset diversity.
36
37
38
39
40
41
42
43
44
45
46
47
48
49
50
51
52
53
54
55
56
57
58
59
60

Repeated Shot Acquisition Scenario

To simulate repeated shot acquisition, field noise recorded at different times was added to the single-shot gathers from the Marmousi model. Three stacking fold numbers (2, 4, and 8) were used as test cases to compare the conventional stacking and our proposed N2NE stacking. In the N2NE framework, the DNNs were trained using pairs of repeated shots. If there were more than two repeated shots, a combination of the two pairs was randomly selected from the sets for each training iteration. The trained DNNs were then applied to repeated shots, and the generated denoised repeated shots were stacked. For comparison, we applied straight stacking and diversity stacking. To quantitatively compare the quality of the denoised results with the corresponding ground truth data, we utilized two performance metrics: the PSNR and structural similarity index measure (SSIM) (Wang et al., 2004). Figure 4 shows the noise attenuation results of N2NE stacking and diversity stacking for various fold numbers. A large amount of high-amplitude tracewise and horizontal noise significantly covered the ground truth signal (Figure 4a). For diversity stacking (Figures 4g-4j), the background noise remained visible even with 16 folds (Figure 4j). However, in N2NE stacking (Figures 4c-4f), the noise was effectively removed by as few as two folds (Figure 4c). The results, including the PSNR and SSIM values,

1
2
3
4 are presented in Table 1. Our proposed N2NE framework consistently improves the PSNR and
5
6
7 SSIM compared with the conventional stacking approach across all test cases.
8
9

10
11 We performed sensitivity analysis based on the size of the training dataset to investigate
12
13
14 the robustness of the proposed method against a limited amount of training data. For this
15
16
17
18 analysis, we prepared datasets with 200, 400, 600, and 800 shot-gather pairs, each with two
19
20
21
22 folds. These shot gathers were extracted from the Marmousi model to decrease the shot point
23
24
25 number rather than through random or equally spaced extraction, assuming that the actual data
26
27
28 acquisition is performed sequentially. The results of the sensitivity analyses are presented in
29
30
31 Table 2. It is evident from the analysis that the size of the shot gather dataset significantly affects
32
33
34 the effectiveness of the N2NE framework, with smaller datasets resulting in reduced denoising.
35
36
37
38 However, even with a small dataset size of 200, the N2NE method outperformed the
39
40
41
42 conventional diversity stack method.
43
44
45

46 **Substack Strategy**

47
48
49

50
51 Thus far, the results have demonstrated that the N2NE framework enhances the denoising
52
53
54 effect compared with conventional stacking methods. However, Table 1 shows that the N2NE
55
56
57
58
59
60

1
2
3
4 framework has limited improvement in the evaluation metrics compared with traditional stacking
5
6
7 methods when the fold number is increased. For example, at a noise level of 0.16, increasing the
8
9
10 fold number from 2 to 16 leads to a PSNR improvement factor of 1.59 with the diversity stack,
11
12
13 whereas the N2NE stack resulted in a more modest improvement factor of 1.08. To improve the
14
15
16 denoising effect of the N2NE stack when a large number of folds are used, we proposed a
17
18
19 substack strategy. In this strategy, instead of directly using pairs of repeated shots to train the
20
21
22 DNN, the shot data were stacked with a small fold number (substack), and the DNN was trained
23
24
25 using pairs of substacked data with noise suppression (Figure 5). The substack was performed at
26
27
28 each iteration of DNN training with a random combination of repeated shots. Figure 6 shows the
29
30
31 results of using the substack strategy with 16 repetitive shots, where the fold numbers utilized for
32
33
34 the substack were 2, 4, and 8. The evaluation metrics improved with the substack strategy,
35
36
37 exhibiting the best results when the number of substack folds was eight. Without the substack
38
39
40 strategy, some reflected waves were damaged (Figure 6c); however, the N2NE stack with the
41
42
43 substack strategy recovered the reflected waves more accurately (Figure 6k). The findings of this
44
45
46 study indicate that integrating the substack strategy into the N2NE framework overcomes the
47
48
49 limited improvements in noise suppression with an increasing number of folds.
50
51
52
53
54
55
56
57
58
59
60

Without Repeated Shot Acquisition Scenario

In the scenarios without denoising, conventional denoising methods were applied within the CRD to generate pseudo-repeat shots. The generated pseudo-denoised shots were then paired with the original shots to train the DNN in the N2NE framework. We employed F-X deconvolution, a median filter, and a blind-trace network (Liu et al., 2023) as the conventional methods. To evaluate the enhanced denoising capability of the N2NE framework, we compared the results of conventional denoising methods with those achieved using the N2NE framework. A distinctive feature of our N2NE framework was that the denoising process used to generate pseudo-noise data occurred in the CRD, which differs from the CSD, where N2N learning occurred. It is expected that learning in different domains will increase the randomness of the noise components in the pseudo-noise and original data. To validate the effectiveness of this approach, we included a case in which N2N learning was conducted in the CRD (both the denoising process and N2N learning were conducted in the same domain) for comparison. In addition, we utilized shot2shot (S2S) with re-de-noising regularization as an N2N-based denoising method for comparison. The hyperparameters of each conventional method were determined using a grid search (Appendix A). The comparison results, including the PSNR and SSIM values, are listed in Table 3. We confirm that the application of our proposed N2NE framework consistently improves the PSNR and SSIM across all conventional methods. Furthermore, our proposed N2NE framework yields better results than a scenario in which the denoising process and N2N learning are performed in the same domain. Figure 7 shows the

1
2
3
4 results of the denoising operation. Although the F-X deconvolution process reduced background
5
6
7 noise to a certain degree, some noise remained (Figure 7c, d). The N2NE framework, trained on
8
9
10 the pseudo-denoised and original data with residual noise, showed that the residual noise was
11
12
13 further reduced, and the PSNR was improved (Figure 7e, f). The Blind-trace network effectively
14
15
16 attenuated the background noise, as shown in Figure 2g. However, the difference plots
17
18
19 demonstrated some degree of ground truth signal leakage (Figure 7h). The Blind-trace network,
20
21
22 enhanced through our proposed N2NE framework, reduced signal leakage while achieving better
23
24
25 noise attenuation (Figure 7i, j). Although our reproduction of the Shot2Shot (S2S) method
26
27
28 effectively suppressed noise in low-noise-level cases, it resulted in artificial gaps and unstable
29
30
31 noise suppression in high-noise-level cases (Figure 7k, l).
32
33
34
35
36
37

DISCUSSION

38
39
40
41
42
43 The proposed N2NE framework used the statistical noise information from the entire
44
45
46 training dataset. Therefore, the volume and diversity of the data were critical factors in
47
48
49 enhancing the accuracy of the proposed N2NE method, as demonstrated by the results of the
50
51
52 sensitivity analysis of the size of the training data in the repeated-shot scenario. Consequently,
53
54
55
56
57
58
59
60

1
2
3
4 although the N2NE framework showed high efficacy in extensive seismic acquisition fields, its
5
6
7 effectiveness is limited to small-scale exploration. Transfer learning can be employed to address
8
9
10 this limitation. Initially, the DNN was trained on synthetic seismic data or datasets from different
11
12
13 regions that provide abundant training data. Subsequently, the weights of the pretrained DNN
14
15
16 were used as initial values to fine-tune the model on a smaller dataset specific to the target
17
18
19 region. The N2NE framework adds DNN training and inference phases to the conventional
20
21
22 denoising method, resulting in a significant computational cost. However, because the
23
24
25 computational cost of the inference phase is relatively low if the models trained under the N2NE
26
27
28 framework have generalization capabilities for data not included in the training phase, such as
29
30
31 data from different surveys, noise suppression might be achievable at a lower computational cost
32
33
34 than existing methods. Evaluating the generalization capabilities of models trained with the
35
36
37 N2NE framework, particularly their effectiveness in transferring knowledge across different
38
39
40 datasets and their potential to reduce computational costs, represents a promising area for future
41
42
43 research. This includes assessing the efficacy of transfer learning within the N2NE framework to
44
45
46 overcome the limitations associated with small data sizes.
47
48
49
50
51
52
53
54
55
56
57
58
59
60

1
2
3 enhanced capability compared with the conventional denoising method. We believe that this
4
5
6
7 study provides a foundation for future research on N2N-based seismic denoising methods and
8
9
10 contributes to improving the quality of seismic records and data acquisition efficiency.
11
12
13

14 DATA AND MATERIALS AVAILABILITY

15
16
17
18
19 Data associated with this research are available and can be accessed via the following

20
21
22
23 URL: <https://zenodo.org/doi/10.5281/zenodo.10663472>
24
25

26 APPENDICES

27 APPENDIX A

28 Hyperparameter search of conventional methods

29
30
31
32
33
34
35 To demonstrate the effectiveness of the proposed Noise2Noise (N2N) enhancement
36
37
38 framework in improving existing noise suppression methods, we used F-X deconvolution, a
39
40
41
42 median filter, and a blind-trace network. Additionally, shot2shot with re-denoising regularization
43
44
45 was used as a comparison method based on the same N2N approach. We determined the
46
47
48 hyperparameters for each method using a grid search, as listed in Table A-1. For F-X
49
50
51
52 deconvolution, implemented in the seismic exploration processing system “SuperX-C”
53
54
55 (manufactured by JGI), we adjusted the spatial operator length of its predictive filter. For the
56
57
58
59
60

1
2
3 median filter implemented in the Python numerical analysis library SciPy (Virtanen et al., 2010),
4
5
6
7 we adjusted the filter length in the temporal and spatial directions. In the blind-trace network
8
9
10 (Liu et al., 2023), we used the same U-net architecture as in the N2NE framework (Figure 3).
11
12
13 The Mean Absolute Error was used as the loss function, and the loss was calculated across the
14
15
16 fully masked trace. The number of noisy traces in the training input data was adjusted as a
17
18
19 hyperparameter.
20
21
22
23
24

25 In our implementation of the S2S framework with re-denoising regularization (Song et
26
27 al., 2023), we used the same U-net architecture as in the N2NE framework. The process involved
28
29
30 adding new noise to the denoising output and then removing it, a process termed "re-denoising."
31
32
33
34 Two penalty terms were introduced: stability (L_{stab}) and re-de-noising terms (L_{rede}), which
35
36
37 together ensured that the denoiser learned as much valid information as possible from the
38
39
40 original image while ensuring that no noise was included in the learned details (For more details,
41
42 refer to Song et al., 2023). According to Song et al. (2023), we used the following loss function:
43
44
45
46
47
48
49

$$L_{denoi} = L_{S2S} + \gamma_1(\gamma_2 L_{rede} + L_{stab}) \quad (A-1)$$

50
51
52
53
54
55
56
57
58
59
60

where γ_1 weighs S2S loss and re-denoising regularization, and γ_2 trades off the re-denoising term and the stability term. We sampled noise from the Poisson distribution for the re-denoising process. In addition, we tuned the γ_1 and the γ_2 as hyperparameters.

Table A-1. The hyperparameter search ranges for various conventional methods.

| Method | Hyperparameter | Range |
|---------------------------------------|-------------------------|------------------------|
| F-X deconvolution | Spatial Operator Length | 3, 5, 7, 9, 11 |
| Median Filter | Spatial Filter Length | 3, 5, 7, 9, 11 |
| | Temporal Filter Length | 3, 5, 7, 9, 11 |
| Blind-trace network | Number of Noisy Traces | 20 %, 40 %, 60 %, 80 % |
| S2S with re-de-noising regularization | γ_1 | 2, 3, 4, 5 |
| | γ_2 | 0.15, 0.25, 0.35, 0.45 |

REFERENCES

Bednar, J. B., 1983, Applications of median filtering to deconvolution, pulse estimation, and statistical editing of seismic data: *Geophysics*, **48**, 1598–1610, doi: 10.1190/1.1441442.

Bekara, M., and M. Van der Baan, 2007, Local singular value decomposition for signal enhancement of seismic data: *GEOPHYSICS*, **72**, V59–V65, doi: 10.1190/1.2435967.

Bekara, M., and M. van der Baan, 2009, Random and coherent noise attenuation by empirical mode decomposition: *GEOPHYSICS*, **74**, V89–V98, doi: 10.1190/1.3157244.

Birnie, C., and M. Ravasi, 2024, Explainable artificial intelligence-driven mask design for self-supervised seismic denoising: *Geophysical Prospecting*, doi: 10.1111/1365-2478.13480.

Birnie, C., M. Ravasi, and T. Alkhalifah, 2021a, Self-supervised learning for random noise suppression in seismic data: First International Meeting for Applied Geoscience & Energy, SEG, Expanded Abstracts, 2869–2873, doi: 10.1190/segam2021-3583248.1.

1
2
3
4 Birnie, C., M. Ravasi, S. Liu, and T. Alkhalifah, 2021b, The potential of self-supervised
5
6
7 networks for random noise suppression in seismic data: *Artificial Intelligence in Geosciences*, **2**,
8
9
10 47–59, doi: 10.1016/j.aiig.2021.11.001.

11
12
13
14 Brusova, O., S. Poche, S. Kainkaryam, A. Valenciano, and A. Sharma, 2021, An
15
16
17 innovative strategy for seismic swell noise removal using deep neural networks, in *First*
18
19
20
21 International Meeting for Applied Geoscience & Energy Expanded Abstracts, Society of
22
23
24 Exploration Geophysicists, 3179–3183, doi: 10.1190/segam2021-3592770.1.

25
26
27
28
29 Canales, L. L., 1984, Random noise reduction, in *SEG Technical Program Expanded*
30
31
32 Abstracts 1984, Society of Exploration Geophysicists, 525–527, doi: 10.1190/1.1894168.

33
34
35
36
37 Chen, Y., M. Zhang, M. Bai, and W. Chen, 2019, Improving the signal - to - noise ratio
38
39
40 of seismological datasets by unsupervised machine learning: *Seismological Research Letters*, **90**,
41
42
43 1552-1564, doi: 10.1785/0220190028.

44
45
46
47
48 Cheng, M., S. Lu, X. Dong, and T. Zhong, 2023a, Multiscale recurrent-guided denoising
49
50
51 network for distributed acoustic sensing-vertical seismic profile background noise attenuation:
52
53
54
55 *GEOPHYSICS*, **88**, WA201–WA217, doi: 10.1190/geo2022-0269.1.

1
2
3 Cheng, S., Z. Cheng, C. Jiang, W. Mao, and Q. Zhang, 2023b, An Effective Self-
4
5
6
7 Supervised Learning Method for Various Seismic Noise Attenuation: arXiv preprint, doi:
8
9
10 10.48550/arXiv.2311.02193.
11
12

13
14
15 Cybenko, G., 1989, Approximation by superpositions of a sigmoidal function:
16
17
18 Mathematics of Control, Signals and Systems, **2**, 303–314, doi: 10.1007/BF02551274.
19
20

21
22
23 Dong, X., Y. Li, and B. Yang, 2019, Desert low-frequency noise suppression by using
24
25
26 adaptive DnCNNs based on the determination of high-order statistic: Geophysical Journal
27
28
29 International, **219**, 1281–1299, doi: 10.1093/gji/ggz363.
30
31

32
33
34 Dong, X., S. Lu, Z. Cong, and T. Zhong, 2023, Multistage residual network for intense
35
36
37 distributed acoustic sensing background noise attenuation: *GEOPHYSICS*, **88**, WC181–WC198,
38
39
40 doi: 10.1190/geo2023-0065.1.
41
42

43
44
45 Fomel, S., and Y. Liu, 2010, Seislet transform and seislet frame: *GEOPHYSICS*, **75**,
46
47
48 V25–V38, doi: 10.1190/1.3380591.
49
50

1
2
3 Gao, J., Z. Li, M. Zhang, Y. Gao, and W. Gao, 2023, Unsupervised Seismic Random
4
5
6
7 Noise Suppression Based on Local Similarity and Replacement Strategy: IEEE Access, 11,
8
9
10 48924–48934, doi: 10.1109/ACCESS.2023.3272905.
11
12

13
14 Gholami, A., 2017, Deconvolutive Radon transform: GEOPHYSICS, 82, V117–V125,
15
16
17
18 doi: 10.1190/geo2016-0377.1.
19
20

21
22 Gulunay, N., 1986, FXDECON and complex wiener prediction filter, in SEG Technical
23
24
25
26 Program Expanded Abstracts 1986, Society of Exploration Geophysicists, 279–281, doi:
27
28
29 10.1190/1.1893128
30
31

32
33
34 Hu, L., X. Zheng, Y. Duan, X. Yan, Y. Hu, and X. Zhang, 2019, First-arrival picking
35
36
37 with a U-net convolutional network: GEOPHYSICS, 84, U45–U57, doi: 10.1190/geo2018-
38
39
40 0688.1.
41
42

43
44
45 Huang, T., S. Li, X. Jia, H. Lu, and J. Liu, 2021, Neighbor2Neighbor: Self-Supervised
46
47
48 Denoising From Single Noisy Images: Proceedings of the IEEE/CVF conference on computer
49
50
51 vision and pattern recognition, 14781–14790, doi: 10.1109/CVPR46437.2021.01454.
52
53
54
55
56
57
58
59
60

1
2
3 Ioffe, S., and C. Szegedy, 2015, Batch Normalization: Accelerating Deep Network
4
5
6
7 Training by Reducing Internal Covariate Shift: Proceedings of the 32nd International Conference
8
9
10 on Machine Learning, 448–456, doi: 10.48550/arXiv.1502.03167.
11
12

13
14 Kingma, D. P., and J. Ba, 2014, Adam: A Method for Stochastic Optimization: arXiv
15
16
17 preprint, doi: 10.48550/arXiv.1412.6980.
18
19
20

21
22 Krull, A., T.-O. Buchholz, and F. Jug, 2019, Noise2Void - Learning Denoising From
23
24
25 Single Noisy Images: 2019 IEEE/CVF Conference on Computer Vision and Pattern Recognition
26
27
28 (CVPR), 2124–2132, doi: 10.1109/CVPR.2019.00223.
29
30
31

32
33 Lapins, S., A. Butcher, J.-M. Kendall, T. S. Hudson, A. L. Stork, M. J. Werner, J.
34
35
36 Gunning, and A. M. Brisbane, 2024, DAS-N2N: machine learning distributed acoustic sensing
37
38
39 (DAS) signal denoising without clean data: Geophysical Journal International, **236**, 1026–1041,
40
41
42 doi: 10.1093/gji/ggad460.
43
44
45
46

47
48 Lehtinen, J., J. Munkberg, J. Hasselgren, S. Laine, T. Karras, M. Aittala, and T. Aila,
49
50
51 2018, Noise2Noise: Learning Image Restoration without Clean Data: Proceedings of the 35th
52
53
54 International Conference on Machine Learning, 2965–2974, doi: 10.48550/arXiv.1803.04189.
55
56
57
58
59
60

1
2
3
4 Li, X., Q. Qi, Y. Yang, P. Duan, and Z. Cao, 2024, Removing abnormal environmental
5
6
7 noise in nodal land seismic data using deep learning: *GEOPHYSICS*, **89**, WA143–WA156, doi:
8
9
10 10.1190/geo2023-0143.1.

11
12
13
14 Liu, D., W. Wang, W. Chen, X. Wang, Y. Zhou, and Z. Shi, 2018, Random-noise
15
16
17 suppression in seismic data: What can deep learning do?: in *SEG Technical Program Expanded*
18
19
20 Abstracts 2018, Society of Exploration Geophysicists, 2016–2020, doi: 10.1190/segam2018-
21
22 2998114.1.

23
24
25
26
27
28 Liu, G.-C., X.-H. Chen, J.-Y. Li, J. Du, and J.-W. Song, 2011, Seismic noise attenuation
29
30
31 using nonstationary polynomial fitting: *Applied Geophysics*, **8**, 18–26, doi: 10.1007/s11770-010-
32
33 0244-2.

34
35
36
37
38
39 Liu, Q., L. Fu, and M. Zhang, 2021, Deep-seismic-prior-based reconstruction of seismic
40
41
42 data using convolutional neural networks: *GEOPHYSICS*, **86**, V131–V142, doi:
43
44
45 10.1190/geo2019-0570.1.
46
47
48
49
50
51
52
53
54
55
56
57
58
59
60

1
2
3
4 Liu, S., C. Birnie, and T. Alkhalifah, 2023, Trace-wise coherent noise suppression via a
5
6
7 self-supervised blind-trace deep-learning scheme: *GEOPHYSICS*, **88**, V459–V472, doi:
8
9
10 10.1190/geo2022-0371.1.
11
12

13
14
15 Lu, W., W. Zhang, and D. Liu, 2006, Local linear coherent noise attenuation based on
16
17
18 local polynomial approximation: *GEOPHYSICS*, **71**, V163–V169, doi: 10.1190/1.2335873
19
20

21
22
23 Luiken, N., M. Ravasi, and C. Birnie, 2024, Integrating self-supervised denoising in
24
25
26 inversion-based seismic deblending: *GEOPHYSICS*, WA39–WA51, doi: 10.1190/geo2023-
27
28
29 0131.1.
30
31

32
33
34 Ma, H., H. Ba, Y. Li, Y. Zhao, and N. Wu, 2023, Unpaired training: Optimize the seismic
35
36
37 data denoising model without paired training data: *GEOPHYSICS*, **88**, WA345–WA360, doi:
38
39
40 10.1190/geo2022-0224.1.
41
42

43
44
45 Mandelli, S., V. Lipari, P. Bestagini, and S. Tubaro, 2019, Interpolation and Denoising of
46
47
48 Seismic Data using Convolutional Neural Networks: arXiv preprint, doi:
49
50
51 10.48550/arXiv.1901.07927.
52
53
54
55
56
57
58
59
60

1
2
3
4 Martin, T., and G. Nash, 2019, Utah FORGE: High-Resolution DAS Microseismic Data
5
6
7 from Well 78-32. United States. <https://dx.doi.org/10.15121/1603679>
8
9

10
11 Moran, N., D. Schmidt, Y. Zhong, and P. Coady, 2020, Noisier2Noise: Learning to
12
13
14
15 Denoise from Unpaired Noisy Data. Proceedings of the IEEE/CVF Conference on Computer
16
17
18 Vision and Pattern Recognition, 12061-12069, doi: 10.1109/CVPR42600.2020.01208
19
20

21
22 Mousavi, S. M., C. A. Langston, and S. P. Horton, 2016, Automatic microseismic
23
24
25
26 denoising and onset detection using the synchrosqueezed continuous wavelet transform:
27
28
29 GEOPHYSICS, **81**, V341–V355, doi: 10.1190/geo2015-0598.1.
30
31

32
33
34 Neelamani, R., A. I. Baumstein, D. G. Gillard, M. T. Hadidi, and W. L. Soroka, 2008,
35
36
37 Coherent and random noise attenuation using the curvelet transform: The Leading Edge, **27**,
38
39
40 240–248, doi: 10.1190/1.2840373.
41
42

43
44
45 Rahaman, N., A. Baratin, D. Arpit, F. Draxler, M. Lin, F. Hamprecht, Y. Bengio, and A.
46
47
48 Courville, 2019, On the Spectral Bias of Neural Networks: Proceedings of the 36th International
49
50
51 Conference on Machine Learning, 5301–5310, doi: 10.48550/arXiv.1806.08734.
52
53
54
55
56
57
58
59
60

1
2
3 Ronneberger, O., P. Fischer, and T. Brox, 2015, U-Net: Convolutional Networks for
4
5
6
7 Biomedical Image Segmentation: Medical Image Computing and Computer-Assisted
8
9
10 Intervention – MICCAI 2015, 234–241, doi: 10.1007/978-3-319-24574-4_28.
11
12

13
14
15 Saad, O. M., and Y. Chen, 2020, Deep denoising autoencoder for seismic random noise
16
17
18 attenuation: *GEOPHYSICS*, **85**, V367–V376, doi: 10.1190/geo2019-0468.1.
19
20

21
22
23 Shan, W., Y. Wang, and W. Lu, 2021, ECA-UNet: Denoise seismic data by learning from
24
25
26 traditional method, in First International Meeting for Applied Geoscience & Energy Expanded
27
28
29 Abstracts, Society of Exploration Geophysicists, 2904–2908, doi: 10.1190/segam2021-
30
31
32 3583394.1.
33
34

35
36
37 Shao, D., Y. Zhao, Y. Li, and T. Li, 2022, Noisy2Noisy: Denoise pre-stack seismic data
38
39
40 without paired training data with labels: *IEEE Geoscience and Remote Sensing Letters*, **19**, 1–5,
41
42
43 doi: 10.1109/LGRS.2022.3145835.
44
45

46
47
48 Song, A., C. Wang, C. Zhang, J. Zhang, X. Wei, and D. Xiong, 2023, Hybrid Shot2Shot
49
50
51 and Re-De-Noising Regularization for Random Noise Attenuation of Seismic Data: *IEEE*
52
53
54
55 *Geoscience and Remote Sensing Letters*, **20**, 1–5, doi: 10.1109/LGRS.2023.3324755.
56
57
58
59
60

1
2
3 Song, H., Y. Gao, W. Chen, Y. Xue, H. Zhang, and X. Zhang, 2020, Seismic random
4
5
6
7 noise suppression using deep convolutional autoencoder neural network: Journal of Applied
8
9
10 Geophysics, **178**, 104071, doi: 10.1016/j.jappgeo.2020.104071.
11
12

13
14 Ulyanov, D., A. Vedaldi, and V. Lempitsky, 2020, Deep Image Prior: International
15
16
17
18 Journal of Computer Vision, **128**, 1867–1888, doi: 10.1007/s11263-020-01303-4.
19
20

21
22 Virtanen, P., R. Gommers, T. E. Oliphant, M. Haberland, T. Reddy, D. Cournapeau, E.
23
24
25
26 Burovski, P. Peterson, W. Weckesser, J. Bright, S. J. van der Walt, M. Brett, J. Wilson, K. J.
27
28
29 Millman, N. Mayorov, A. R. J. Nelson, E. Jones, R. Kern, E. Larson, C. J. Carey, Í. Polat, Y.
30
31
32 Feng, E. W. Moore, J. VanderPlas, D. Laxalde, J. Perktold, R. Cimrman, I. Henriksen, E. A.
33
34
35
36 Quintero, C. R. Harris, A. M. Archibald, A. H. Ribeiro, F. Pedregosa, and P. van Mulbregt,
37
38
39 2020, SciPy 1.0: fundamental algorithms for scientific computing in Python: Nature Methods,
40
41
42
43 **17**, 261–272, doi: 10.1038/s41592-019-0686-2
44
45

46
47 Wang, H., and J. Zhang, 2021, Seismic noise attenuation by applying a deep learning
48
49
50
51 method without noise-free labels, in First International Meeting for Applied Geoscience &
52
53
54
55
56
57
58
59
60

1 Geophysics

36

2
3 Energy Expanded Abstracts, Society of Exploration Geophysicists, 2909–2913, doi:

4
5
6
7 10.1190/segam2021-3583901.1.

8
9
10
11 Wang, R., R. Zhang, C. Bao, L. Qiu, and D. Yang, 2022, Adapting the residual dense
12 network for seismic data denoising and upscaling: *GEOPHYSICS*, **87**, V321–V340, doi:

13
14
15
16
17
18 10.1190/geo2021-0294.1.

19
20
21
22 Wang, T., M. Zhang, Q. Yu, and H. Zhang, 2012, Comparing the applications of EMD
23 and EEMD on time–frequency analysis of seismic signal: *Journal of Applied Geophysics*, **83**,
24
25
26
27
28
29
30 29–34, doi: 10.1016/j.jappgeo.2012.05.002.

31
32
33
34 Wang, X., S. Fan, C. Zhao, D. Liu, and W. Chen, 2023, A Self-Supervised Method Using
35
36
37
38
39
40
41
42
43
44
45
46
47
48
49
50
51
52
53
54
55
56
57
58
59
60
Noise2Noise Strategy for Denoising CRP Gathers: *IEEE Geoscience and Remote Sensing
Letters*, **20**, 1–5, doi: 10.1109/LGRS.2023.3285951.

54
55
56
57
58
59
60
Wang, Y., W. lu, J. Liu, M. Zhang, and Y. Miao, 2019, Random seismic noise
attenuation based on data augmentation and CNN: *Acta Geophysica Sinica*, **62**, 421–433, doi:
10.6038/cjg2019M0385.

1
2
3
4 Wang, Z., A. C. Bovik, H. R. Sheikh, and E. P. Simoncelli, 2004, Image quality
5
6
7 assessment: from error visibility to structural similarity: IEEE Transactions on Image Processing,
8
9
10 **13**, 600–612, doi: 10.1109/TIP.2003.819861.

11
12
13
14 Xiong, W., X. Ji, Y. Ma, Y. Wang, N. M. AlBinHassan, M. N. Ali, and Y. Luo, 2018,
15
16
17 Seismic fault detection with convolutional neural network: GEOPHYSICS, **83**, O97–O103, doi:
18
19
20 10.1190/geo2017-0666.1.
21
22

23
24
25
26 Xu, Z.-Q. J., Y. Zhang, T. Luo, Y. Xiao, and Z. Ma, 2020, Frequency Principle: Fourier
27
28
29 Analysis Sheds Light on Deep Neural Networks: Communications in Computational Physics, **28**,
30
31
32 1746–1767, doi: 10.4208/cicp.OA-2020-0085.
33
34

35
36
37 Yang, F., and J. Ma, 2019, Deep-learning inversion: A next-generation seismic velocity
38
39
40 model building method: GEOPHYSICS, **84**, R583–R599, doi: 10.1190/geo2018-0249.1.
41
42
43

44
45 Yang, L., S. Fomel, S. Wang, X. Chen, Y. Chen, and Y. Chen, 2023, SLKNet: An
46
47
48 attention-based deep-learning framework for downhole distributed acoustic sensing data
49
50
51 denoising: GEOPHYSICS, **88**, WC69–WC89, doi: 10.1190/geo2022-0724.1.
52
53
54
55
56
57
58
59
60

1
2
3 Yu, S., J. Ma, and W. Wang, 2019, Deep learning for denoising: *GEOPHYSICS*, **84**,
4 V333–V350, doi: 10.1190/geo2018-0668.1.
5
6
7

8
9
10
11 Zhang, M., Y. Liu, M. Bai, and Y. Chen, 2019b, Seismic Noise Attenuation Using
12 Unsupervised Sparse Feature Learning: *IEEE Transactions on Geoscience and Remote Sensing*,
13
14
15
16
17
18 **57**, 9709–9723, doi: 10.1109/TGRS.2019.2928715.
19
20

21
22 Zhang, Y., D. Li, K. L. Law, X. Wang, H. Qin, and H. Li, 2022, IDR: Self-Supervised
23 Image Denoising via Iterative Data Refinement: 2022 IEEE/CVF Conference on Computer
24
25
26
27
28
29
30
31
32
33
34
35
36
37
38
39
40
41
42
43
44
45
46
47
48
49
50
51
52
53
54
55
56
57
58
59
60

29 Vision and Pattern Recognition (CVPR), 2088–2097, doi: 10.1109/CVPR52688.2022.00214.
30
31
32
33
34 Zhang, Y., and B. Wang, 2023, Unsupervised seismic random noise attenuation by a
35
36
37
38
39
40
41
42
43
44
45
46
47
48
49
50
51
52
53
54
55
56
57
58
59
60

41
42
43
44
45
46
47
48
49
50
51
52
53
54
55
56
57
58
59
60

1
2
3
4 Zhao, Y., Y. Li, X. Dong, and B. Yang, 2018, Low-Frequency Noise Suppression
5
6
7 Method Based on Improved DnCNN in Desert Seismic Data: IEEE Geoscience and Remote
8
9
10 Sensing Letters, 1–5, doi: 10.1109/LGRS.2018.2882058.
11
12

13
14 Zhu, L., E. Liu, and J. H. McClellan, 2015, Seismic data denoising through multiscale
15
16
17 and sparsity-promoting dictionary learning: GEOPHYSICS, **80**, WD45–WD57,
18
19
20
21 10.1190/geo2015-0047.1.
22
23
24
25
26
27
28
29
30
31
32
33
34
35
36
37
38
39
40
41
42
43
44
45
46
47
48
49
50
51
52
53
54
55
56
57
58
59
60

LIST OF FIGURES

1
2
3
4
5
6
7
8
9
10
11
12
13
14
15
16
17
18
19
20
21
22
23
24
25
26
27
28
29
30
31
32
33
34
35
36
37
38
39
40
41
42
43
44
45
46
47
48
49
50
51
52
53
54
55
56
57
58
59
60

Figure 1. Flowchart of conventional (a) and N2NE stacks (b) under a repeated shot scenario.

Figure 2. Flowchart of N2NE framework without a repeated shot scenario.

Figure 3. Schematic U-net architecture in this study. The integer number represents the number of feature maps of convolution layers. Except for the last convolution layer, the convolution outputs were applied for batch normalization and passed through a ReLU. Final output passing through the sigmoid layer to be normalized.

Figure 4. Denoising results under a repeated shot scenario. (a) Noisy shot gather. (b) Ground truth shot gather. (c-f) N2NE stack results with different fold numbers. (g-j) Diversity stack results with different fold numbers.

Figure 5. Flowchart of N2NE stack with the substack strategy.

Figure 6. Denoising results of different stack methods with 16 repetitive shots. (a) Noisy shot gather. (b) Ground truth shot gather. Denoising results and signal leakage of N2NE stack without substack (c, d), diversity stack (e, f), and N2NE stack with different substack fold numbers (g-l), respectively. The areas within the red dotted rectangles are shown enlarged.

Figure 7. Denoising results in the absence of repeated shot scenarios. (a) Noisy shot gather. (b) Ground truth shot gather. Denoising results and signal leakage by F-X deconvolution (c, d), N2NE F-X deconvolution (e, f), Blind Trace Network (g, h), N2N Blind Trace Network (i, j), and Shot2Shot with Re-denoising Regularization (k, l). The areas within the red dotted rectangles are shown enlarged.

LIST OF TABLES

Table 1. Evaluation metrics (PSNR/SSIM) comparison of stacking methods under repeated shots scenario. Bold indicates the highest evaluation metrics.

Table 2. Evaluation metrics (PSNR/SSIM) comparison of N2NE stacking methods under different data sizes.

Table 3. Evaluation metrics (PSNR/SSIM) comparison for conventional denoising methods, with and without the N2NE framework, as well as the S2S method, in a repeated shots scenario.

N2NE(CRD) means the case of N2N learning is conducted in CRD. Bold indicates the highest evaluation metrics, while underscore denotes the highest metrics among identical conventional methods.

Table 1. Evaluation metrics (PSNR/SSIM) comparison of stacking methods under repeated shots scenario. Bold indicates the highest evaluation metrics.

| Noise Scale | Fold Number | Normal Stack | Diversity Stack | N2NE Stack |
|-------------|-------------|--------------|-----------------|--------------------|
| 0.02 | 2 | 33.23/0.940 | 35.08/0.923 | 42.68/0.987 |
| | 4 | 35.99/0.966 | 38.52/0.960 | 44.56/0.992 |
| | 8 | 38.93/0.977 | 41.73/0.980 | 45.81/0.993 |
| | 16 | 42.32/0.986 | 44.89/0.990 | 46.24/0.994 |
| 0.04 | 2 | 27.21/0.877 | 29.13/0.797 | 38.32/0.961 |
| | 4 | 29.97/0.931 | 32.63/0.875 | 40.05/0.975 |
| | 8 | 32.91/0.946 | 35.87/0.930 | 42.13/0.984 |
| | 16 | 36.30/0.958 | 39.08/0.963 | 41.71/0.982 |
| 0.08 | 2 | 21.19/0.846 | 23.15/0.700 | 35.56/0.926 |
| | 4 | 23.94/0.903 | 26.69/0.704 | 37.24/0.949 |
| | 8 | 26.89/0.909 | 29.95/0.800 | 37.17/0.949 |
| | 16 | 30.28/0.908 | 33.20/0.879 | 38.45/0.961 |
| 0.16 | 2 | 15.17/0.837 | 17.15/0.677 | 33.10/0.874 |
| | 4 | 17.92/0.895 | 20.71/0.610 | 34.38/0.906 |
| | 8 | 20.87/0.892 | 23.98/0.606 | 34.64/0.912 |
| | 16 | 24.26/0.863 | 27.26/0.690 | 35.68/0.930 |

1
2
3
4
5
6
7
8
9
10
11
12
13
14
15
16
17
18
19
20
21
22
23
24
25
26
27
28
29
30
31
32
33
34
35
36
37
38
39
40
41
42
43
44
45
46
47
48
49
50
51
52
53
54
55
56
57
58
59
60

Table 2. Evaluation metrics (PSNR/SSIM) comparison of N2NE stacking methods under different data sizes.

| NoiseLevel | Data Size | | |
|------------|-------------|-------------|-------------|
| | 200 | 400 | 801 |
| 0.02 | 36.63/0.967 | 39.37/0.98 | 44.15/0.989 |
| 0.04 | 34.76/0.942 | 37.22/0.963 | 38.32/0.961 |
| 0.08 | 32.87/0.894 | 35.05/0.934 | 35.56/0.926 |
| 0.16 | 29.62/0.717 | 30.08/0.756 | 33.1/0.874 |

For Peer Review

Geophysics

44

Table 3. Evaluation metrics (PSNR/SSIM) comparison for conventional denoising methods, with and without the N2NE framework, as well as the S2S method, in a repeated shots scenario.

N2NE(CRD) means the case of N2N learning is conducted in CRD. Bold indicates the highest evaluation metrics, while underscore denotes the highest metrics among identical conventional methods.

| Noise Scale | 0.02 | 0.04 | 0.08 |
|---------------------------------------|----------------------------|---------------------------|---------------------------|
| Original Noisy Shot | 30.93/0.885 | 24.91/0.807 | 18.89/0.788 |
| F-X-deconvolution | 38.36/0.967 | 33.59/0.901 | 28.41/0.761 |
| N2NE F-X deconvolution (Proposed) | <u>41.68/0.979</u> | <u>37.91/0.948</u> | <u>33.72/0.865</u> |
| N2NE F-X deconvolution (CRD) | 41.21/ <u>0.979</u> | 37.58/0.945 | 33.48/0.856 |
| Median Filter | 34.17/0.920 | 31.71/0.819 | 27.68/0.673 |
| N2NE median Filter (Proposed) | <u>35.30/0.948</u> | <u>33.76/0.890</u> | <u>31.02/0.751</u> |
| N2NE median Filter (CRD) | 34.74/0.931 | 32.45/0.838 | 28.74/0.675 |
| Blind-trace network | 38.53/0.971 | 36.73/0.956 | 33.66/0.924 |
| N2NE blind-trace network (Proposed) | <u>40.21/0.977</u> | <u>38.08/0.962</u> | <u>35.07/0.937</u> |
| N2NE blind-trace network (CRD) | 39.49/0.975 | 37.73/0.960 | 34.99/0.935 |
| S2S with re-de-noising regularization | 39.34/0.970 | 35.62/0.922 | 31.67/0.840 |

1
2
3
4
5
6
7
8
9
10
11
12
13
14
15
16
17
18
19
20
21
22
23
24
25
26
27
28
29
30
31
32
33
34
35
36
37
38
39
40
41
42
43
44
45
46
47
48
49
50
51
52
53
54
55
56
57
58
59
60

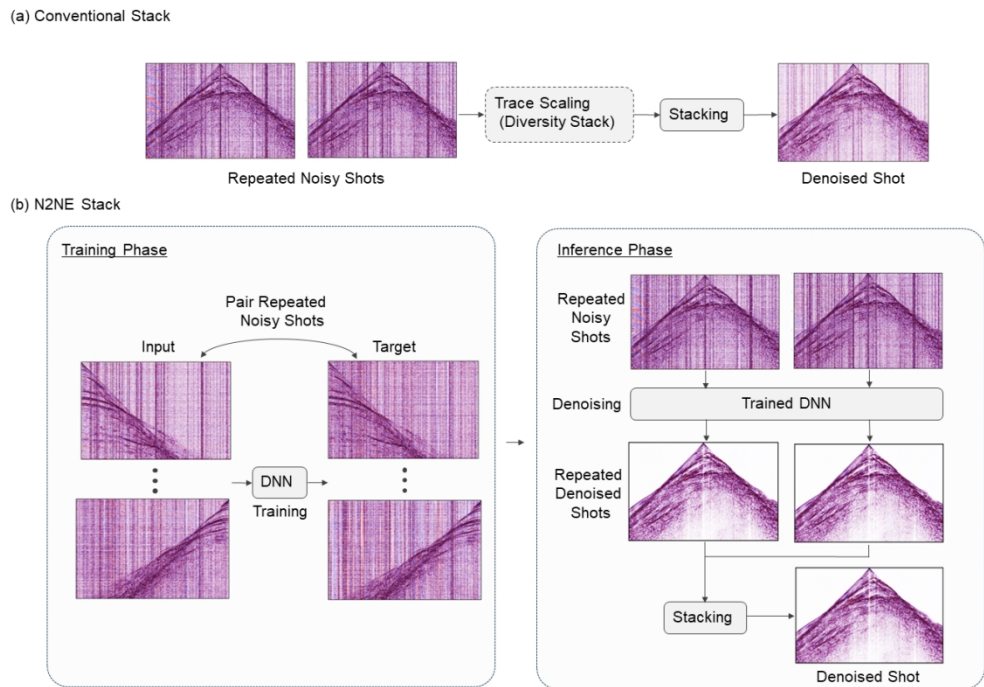


Figure 1. Flowchart of conventional (a) and N2NE stacks (b) under a repeated shot scenario.

898x673mm (38 x 38 DPI)

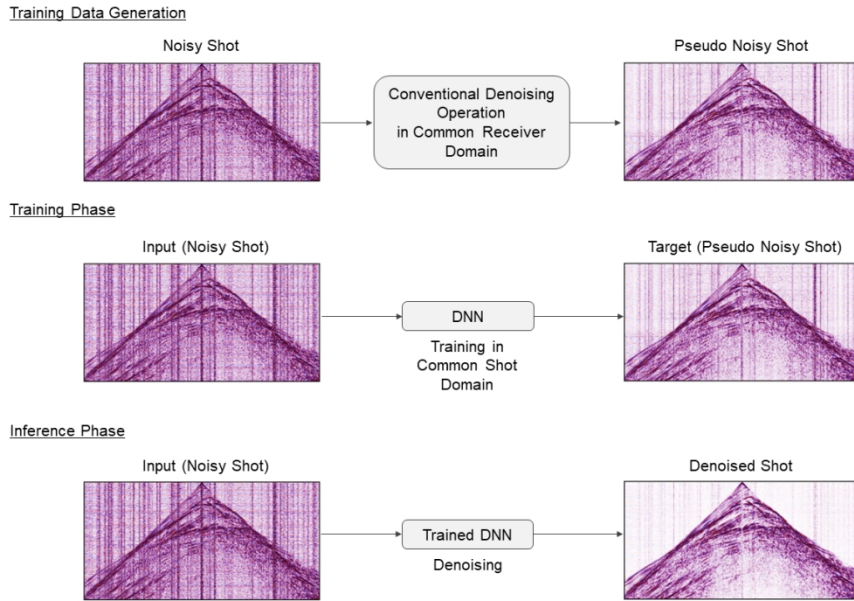


Figure 2. Flowchart of N2NE framework without a repeated shot scenario.

898x673mm (38 x 38 DPI)

1
2
3
4
5
6
7
8
9
10
11
12
13
14
15
16
17
18
19
20
21
22
23
24
25
26
27
28
29
30
31
32
33
34
35
36
37
38
39
40
41
42
43
44
45
46
47
48
49
50
51
52
53
54
55
56
57
58
59
60

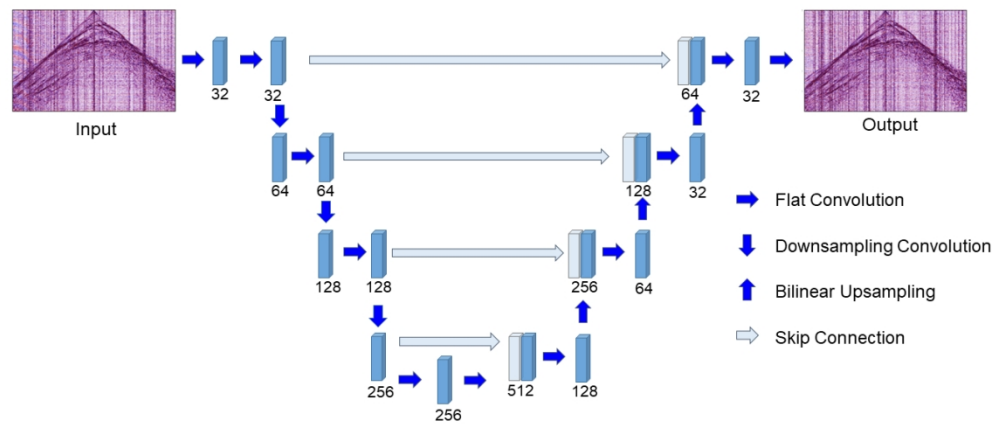


Figure 3. Schematic U-net architecture in this study. The integer number represents the number of feature maps of convolution layers. Except for the last convolution layer, the convolution outputs were applied for batch normalization and passed through a ReLU. Final output passing through the sigmoid layer to be normalized.

898x673mm (38 x 38 DPI)

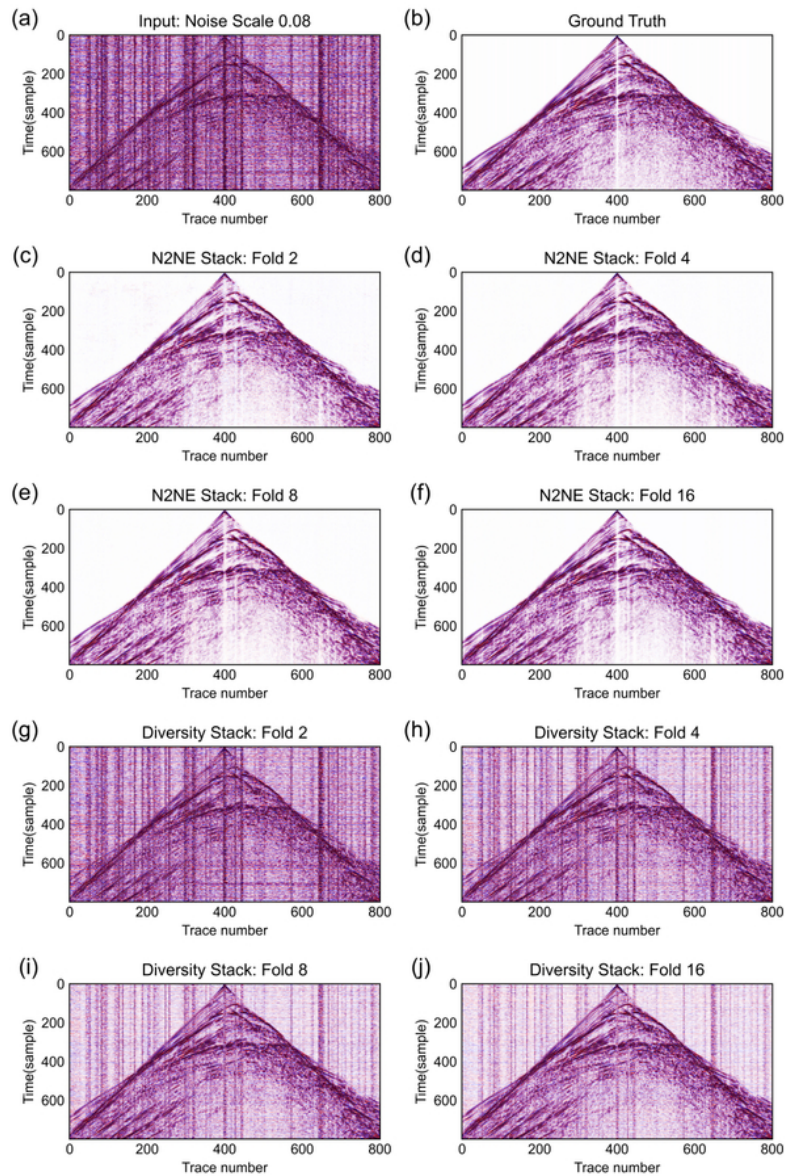


Figure 4. Denoising results under a repeated shot scenario. (a) Noisy shot gather. (b) Ground truth shot gather. (c-f) N2NE stack results with different fold numbers. (g-j) Diversity stack results with different fold numbers.

51x77mm (300 x 300 DPI)

1
2
3
4
5
6
7
8
9
10
11
12
13
14
15
16
17
18
19
20
21
22
23
24
25
26
27
28
29
30
31
32
33
34
35
36
37
38
39
40
41
42
43
44
45
46
47
48
49
50
51
52
53
54
55
56
57
58
59
60

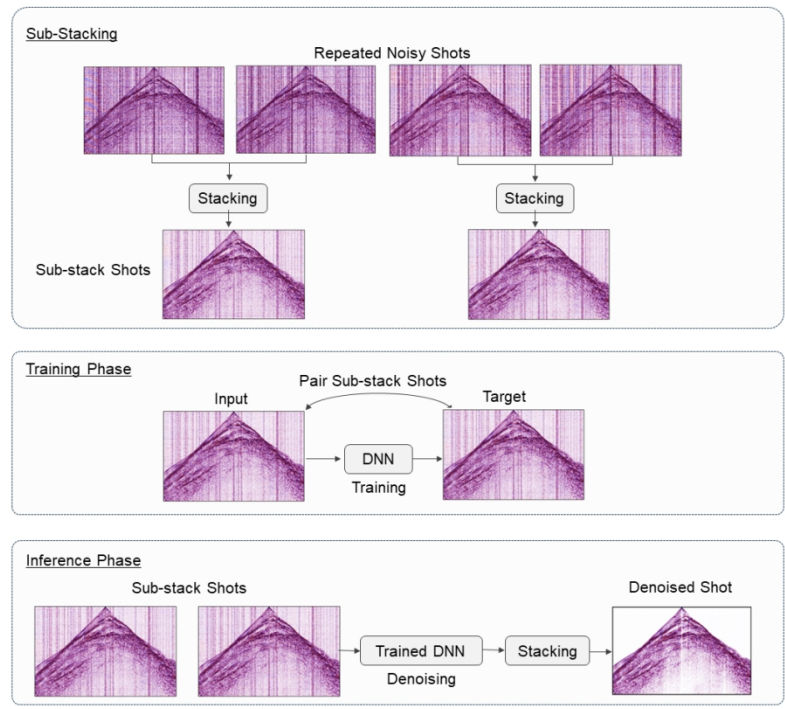


Figure 5. Flowchart of N2NE stack with the substack strategy.

898x673mm (38 x 38 DPI)

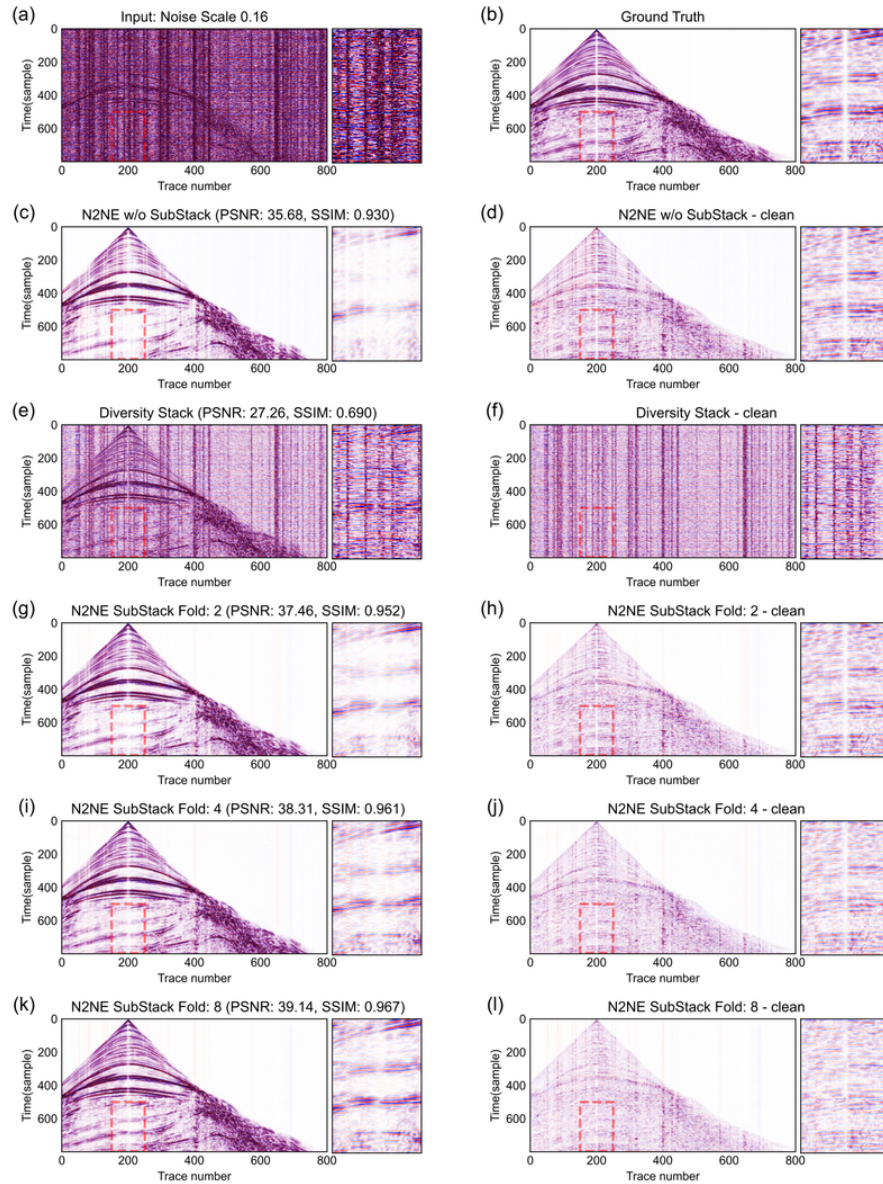


Figure 6. Denoising results of different stack methods with 16 repetitive shots. (a) Noisy shot gather. (b) Ground truth shot gather. Denoising results and signal leakage of N2NE stack without substack (c, d), diversity stack (e, f), and N2NE stack with different substack fold numbers(g-l), respectively. The areas within the red dotted rectangles are shown enlarged.

74x90mm (300 x 300 DPI)

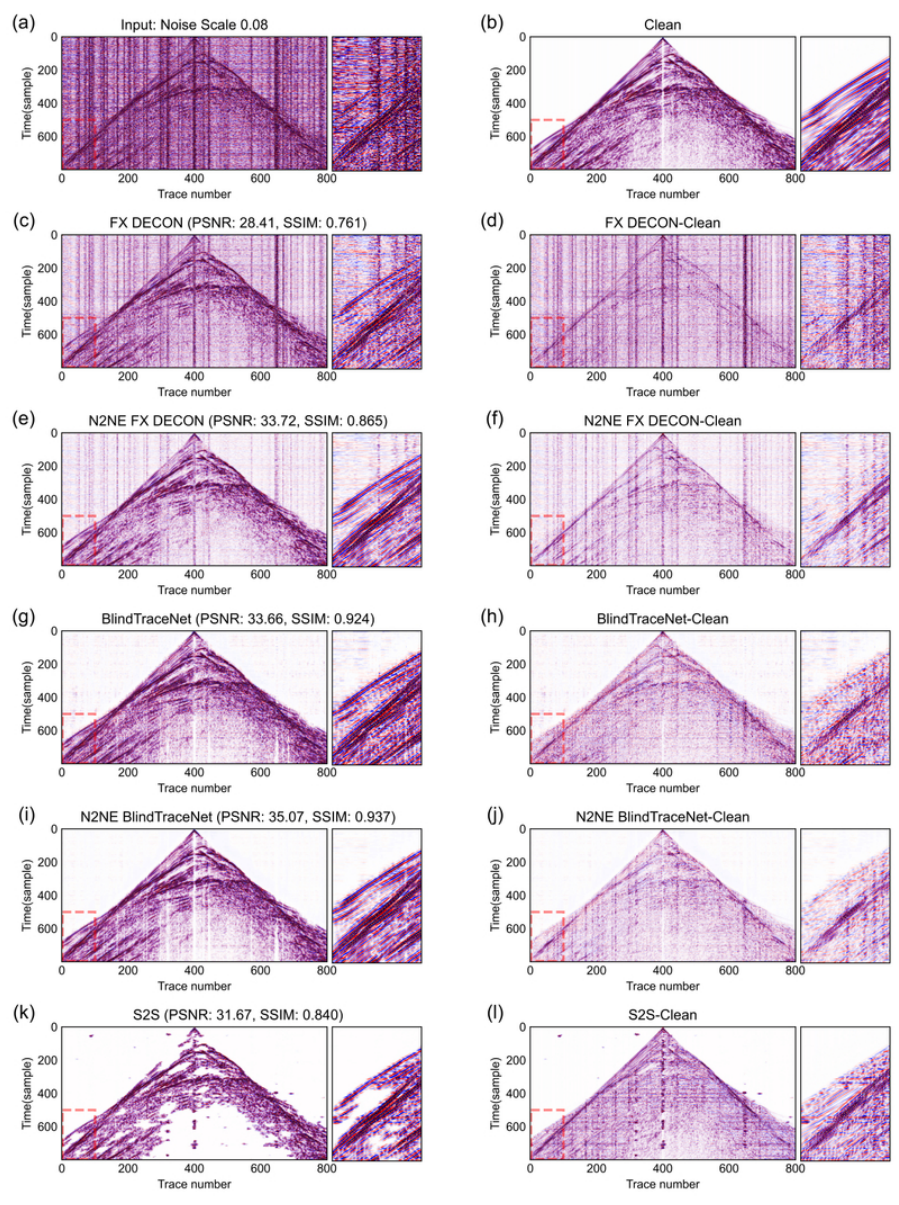


Figure 7. Denoising results in the absence of repeated shot scenarios. (a) Noisy shot gather. (b) Ground truth shot gather. Denoising results and signal leakage by F-X deconvolution (c, d), N2NE F-X deconvolution (e, f), Blind Trace Network (g, h), N2N Blind Trace Network (i, j), and Shot2Shot with Re-denoising Regularization (k, l). The areas within the red dotted rectangles are shown enlarged.

74x90mm (300 x 300 DPI)